Redesign of Rotor Can for Hermetically Sealed Pump by Use of Composite Material

A. C. Sørensen, M. A. Fremmelev, M. Balleby, O. Nielsen, P. Olesen and R. F. B. Andersen

Department of Materials and Production, Aalborg University
Fibigerstraede 16, DK-9220 Aalborg East, Denmark
Email: {acsa14, mfremm13, mballe14, oniels14, polese14, rfba14}@student.aau.dk,
Web page: http://www.mechman.m-tech.aau.dk/

Abstract
This paper is concerned with optimal design of a rotor can, which is part of the Grundfos MAGdrive system used to hermetically seal pumps. The existing stainless steel rotor can is analyzed to yield understanding of the system behaviour. Subsequently, a conceptual redesign of a composite rotor can is conducted. Hence, the fixation is redesigned and the rotor can is to be mounted by use of an adhesive joint. The properties of the adhesive joint are investigated by use of uniaxial tensile testing. The prototype used for tensile testing is used to validate a corresponding FE model. On the basis of the experimental results, a design for the full-size model adhesive joint is established. An ANSYS finite element model is used in combination with MATLAB optimization algorithms to minimize the mass of the rotor can. This is done by use of the following variables: number of layers, layer thickness and fiber orientation as well as the shape of the rotor can top. Additionally, the model is subject to stiffness, strength, geometrical and manufacturing constraints.

Keywords: Composite shell, Adhesive joint, Constrained optimization

1. Introduction

The problem has been formulated by Grundfos with the desire to redesign the rotor can, marked red in Fig. 1. The aim is to reduce manufacturing costs and increase efficiency of the magnetic drive. On that basis, the following research question is defined:

Can a composite rotor can be designed to replace the existing stainless steel rotor can to achieve lower manufacturing costs and gain increased efficiency of the MAGdrive system, albeit when subjected to altered requirements regarding applied loading?

To serve as a basis for the redesign of the rotor can, the existing solution is examined.

1.1 Presentation of Existing Rotor Can

A section cut of the MAGdrive system is illustrated in Fig. 1, including denomination of the numbered components in Tab. I.

1	2	3	4	5	6	7	8
Rotor Can	Inner Drive	Outer Drive	Pumped Media	Magnets	Manacle Ring	Bearing Housing	Seal

Tab. I Denominations used for Fig. 1.

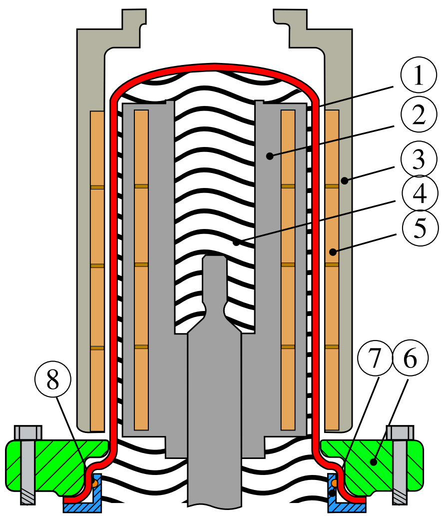

Fig. 1 Conceptual illustration of the MAGdrive system. The wave-pattern illustrates the pumped media.

The rotor can is fixed between the bearing housing and manacle ring, with the manacle ring being fastened with pretensioned bolts.

1.2 Finite Element Analysis of Existing Rotor Can

The boundary conditions (BCs) applied to the model are illustrated by a conceptual drawing in Fig. 2.

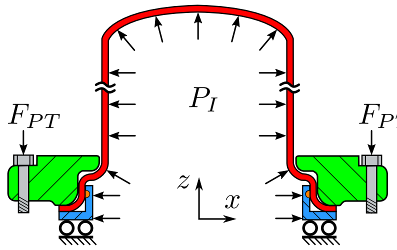

Fig. 2 Conceptual illustration of applied BCs. P_I is the internal fluid pressure, F_{PT} is the bolt pretension force.

The global coordinate system is defined as follows: The x- and y-axis are oriented in the radial direction of the rotor can. The z-axis is aligned with the axial direction of the cylindrical part of the rotor can. A 3D model of the rotor can is created and evaluated in ANSYS Workbench. For the discretization, 3D solid elements with quadratic interpolation functions are used. Applied BCs include the following: All degrees of freedom (DOF) of the bolt threads are locked. Displacements of the bearing housing are locked in the z-direction, applied to the bottom face of the bearing housing. The applied BCs are listed in Tab. II:

Description	Value
Internal pressure [MPa]	2.5
Bolt pretension [N]	4400
Bolt fixation [mm]	$u = v = w = 0$
Bearing housing fixation [mm]	$w = 0$
Rotation of symmetry faces [°]	$\phi_z = 0$

Tab. II BCs applied to the model. u, v and w refer to displacement in the x-, y- and z-direction respectively. ϕ_z refers to rotation about the z-axis.

The BC $\phi_z = 0°$, locking rotation of symmetry faces, is defined with respect to a local cylindrical coordinate system. The local cylindrical coordinate system is shown in Fig. 3 in the center of the rotor can model shown in section view.

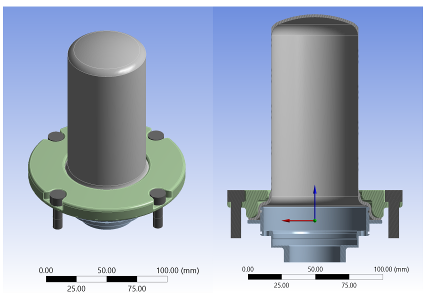

Fig. 3 Isometric and section view of the existing rotor can.

Contact elements are used to model the faces where the rotor can is in contact with the bearing housing or manacle ring. To model contact behaviour, the Augmented Lagrange formulation is chosen. This formulation is a combination of the penalty method and the Lagrange multiplier method, as described in [1]. The penalty method adds large artificial stiffnesses if two bodies are in contact. The Lagrange multiplier method introduces additional variables, used to describe the kinematic conditions of the contact behaviour. In this case, the kinematic conditions could be no penetration of bodies. The Augmented Lagrange formulation utilizes parts of the two mentioned formulations and yields good convergence properties. Asymmetric contact formulation is selected, yielding node-to-line contact. Thus, lines from the target surface and nodes from the contact surface are used to model the contact behaviour. The rotor can is discretized with a finer mesh than the other components. Hence, its faces are selected as contact surfaces, while surfaces on the bearing housing and manacle ring are selected as target surfaces. To account for non-linear contact behavior, large displacements are enabled. Thus, a non-linear finite element analysis (FEA) is conducted. The cyclic symmetry of the assembly is utilized, and the size of the model is thus reduced to one eighth of the full model, shown in Fig. 4.

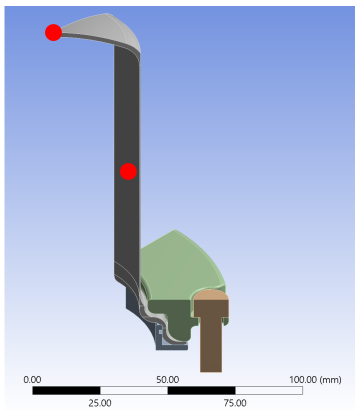

Fig. 4 Reduced model. The radially cut faces are denominated symmetry faces. The red dots mark the points at which displacements and stresses listed in Tab. IV are calculated. The points are denominated top point and midpoint.

A convergence study of displacements is conducted to determine a sufficient mesh quality, yielding an element length of 1 mm. This results in approximately 8×10^4 nodes in the rotor can. In addition to the convergence study, the model is validated as follows: The reaction forces in the model are compared to analytical calculations of the force components resulting from the applied pressure, yielding a difference of 0.2%. Furthermore, solutions from mechanics of materials (MoM) to the normal axial (σ_a) and hoop stresses

(σ_h) in thin-walled pressure vessels are compared to the stresses in the illustrated points in the model. The stresses calculated from the FEA and the MoM approach are shown in Tab. III:

	MoM	FEA	Deviation [%]
σ_h [MPa]	200.0	198.5	0.7
σ_a [MPa]	100.0	99.2	0.8

Tab. III Comparison of MoM and FEA solutions.

Results from the FEA are summarized in Tab. IV.

Description	Value	Unit
Deformation		
Max. axial deformation of top point	0.179	mm
Max. radial deformation at midpoint	0.034	mm
Stress		
Axial stress at midpoint	99.2	MPa
Hoop stress at midpoint	198.5	MPa
Meridional stress at top point	70.8	MPa
Strain		
Max. equivalent total strain	0.13	%

Tab. IV Results from the FEA.

On the basis of the results presented above, the existing rotor can does not fail due to static failure.

1.3 Requirements for Rotor Can Redesign

The following requirements are defined for maximal displacement, relating to the existing rotor can dimensions:

- $\{u_{max}\ ,\ v_{max}\} \leq 0.15$ mm
- $w_{max} \leq 1.5$ mm

As proposed by Grundfos, the internal pressure and the temperature range are altered compared to the existing solution. This is done with the purpose of obtaining a lower-cost design:

- Internal pressure: $P_I = 1$ MPa
- Temperature range: $-40°\mathrm{C} \leq T \leq 70°\mathrm{C}$

For the conducted calculations, a safety factor has been applied to the internal pressure. Due to confidentiality, the safety factor is not listed.
Regarding rotor can thickness, geometrical limitations are present. From the conducted FEA, relatively large stresses have been shown to result in the existing design. Based on the requirements for maximal displacement, high stiffness is required. This makes the use of a high strength composite material like a carbon fiber reinforced polymer (CFRP) favourable. From a functionality point of view, the new design should provide hermetic sealing. The utilized material is changed from a material which is isotropic and linear elastic to one which is a generally orthotropic and viscoelastic. Thus, re-evaluation of the design is required.

1.4 Definition of New Design Concept

A methodological design approach is used to generate a number of possible designs, using the following steps:

- Establishment of rotor can functions
- Generation of concepts
- Reduction of solution space
- Selection of final concept

The chosen functions are fixation and manufacturing, and the considered function solutions are as follows:

- Fixation: Clamped, bonded, bolted and geometric.
- Manufacturing: Prepreg compression moulding, filament winding and injection moulding with discontinuous fibers.

In addition to the solution space created by the above functions, two hybrid concepts are included: A steel hybrid and a polymer hybrid. The steel hybrid utilizes the fixation from the existing rotor can, to which a composite rotor can is adhered. The polymer hybrid consists of an internal part made of polymer, around which a composite is wound. The chosen final concept is shown in Fig. 5.

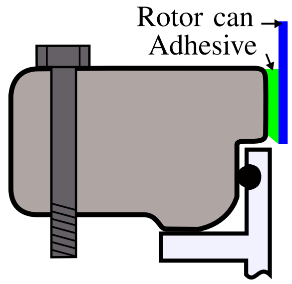

Fig. 5 Conceptual illustration of selected design concept.

Thus, the rotor can should be fixed to the manacle ring by use of an adhesive, requiring the design of the adhesive joint. Due to the chosen fixation, the entire bottom part of the rotor can may be cylindrical. Filament winding may thus be used as a manufacturing process for the entire rotor can.
A comparison of various materials has been conducted to select a fiber reinforced polymer and an adhesive. The selected materials are a carbon fiber reinforced epoxy (CFRE) and an epoxy adhesive.

2. Methods

In the following, the methods utilized to design the composite rotor can and the adhesive joint are presented.

2.1 Design of Adhesive Joint

Due to the shape of the rotor can and manacle ring, the adhesive joint is a tubular single lap joint. Flat and tubular single lap joints are shown in Fig. 6.

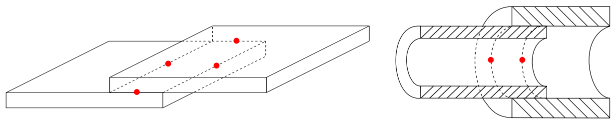

Fig. 6 Illustration of flat and tubular single lap joints, with a section cut shown of the tubular joint. The red dots indicate edges with stress concentrations.

As shown on the above figure, stress concentrations are present at the edges of the adhesive. Fewer edges are present for a tubular joint than for a flat joint. This entails fewer edges with stress concentrations in the adhesive, also denominated edge effects. For the selected epoxy adhesive, material data is available for a single lap joint, which might not be valid for a tubular lap joint. Thus, experiments are conducted to compare the listed failure strength for a flat single lap joint to that obtained by a tubular single lap joint.

2.1.1 Experimental Estimation of Material Data

To estimate the failure strength of the rotor can adhesive joint, test specimens are manufactured. These consist of CFRE tubes, which are adhered to steel fixations by use of an epoxy adhesive. Mechanical properties of the adhesive are shown in Tab. V.

Modulus of elasticity	1.9 GPa
Adhesive shear strength	35 MPa
Steel interface shear strength	*25 MPa
CFRE interface shear strength	19 MPa

Tab. V Adhesive properties based on [2]. * refers to the interface strength of a sandblasted surface.

The test specimen is shown in Fig. 7. Red teflon tape is applied to the ends of the CFRE tube at distance of 16 mm from the tube ends to accurately control the adhesive length.

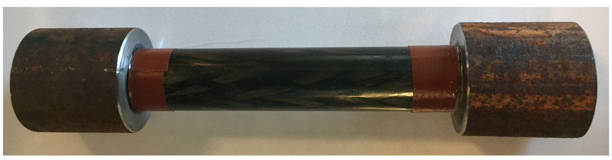

Fig. 7 Test specimen.

To determine the static failure strength of the adhesive joint, uniaxial tensile testing is performed. The measured results are plotted in Fig. 8, where the dotted line represents the mean failure value of 21.6 kN.
Test samples 1, 3, 5 and 6 have been dismissed as outliers due to inadequate adhesive finish. This was established from review of the fractured test specimens, where large areas with no adhesive applied to the adherends were clearly visible. This most likely stemmed from air trapped within the adhesive.

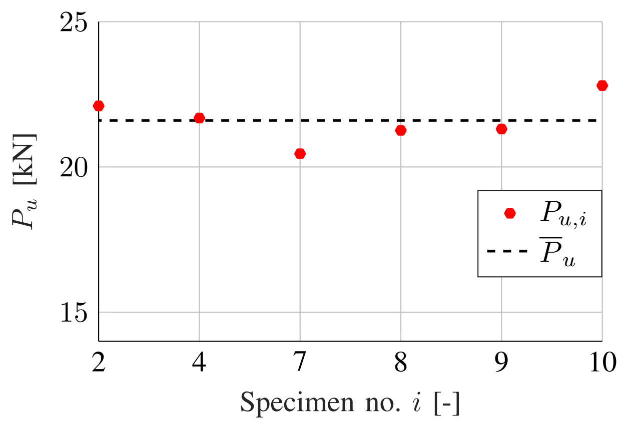

Fig. 8 Results from tensile tests with test specimens. P_u is the ultimate tensile force, $P_{u,i}$ is the ultimate tensile force measured for the i^{th} test specimen. The overline in $\overline{P}_u$ refers to the mean value, being equal to 21.6 kN.

The experimental results are compared to an ANSYS model of the adhesive joint, shown in Fig. 9. A tensile load equal to the experimentally determined mean value of the failure load is applied to the model. From the model, the shear stress in each adhesive-adherend interface exceeds the associated interface strength limit, as listed in Tab. V. Hence, failure is expected to occur at one of the adhesive-adherend interfaces.

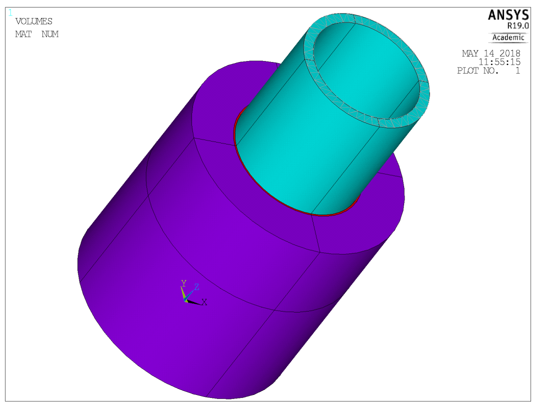

Fig. 9 ANSYS model of adhesive joint. The steel fixation and CFRE tube are shown purple and blue respectively.

Tab. VI shows the dimensions of the test specimens.

r_i	r_o	l_a	t_a	t_s
10	11.85	16	0.3	8

Tab. VI Dimensions [mm] of the test specimen. r_i and r_o are the inner and outer radius of the tube respectively, l_a and t_a are the length and thickness of the adhesive respectively, and t_s is the wall thickness of the steel fixation.

By visual inspection of the test specimens, failure was seen to occur at the steel interface. This is deemed to originate from a lower interface strength of the milled steel surface, which differs from that shown in Tab. V. Overall, the ANSYS model predicted failure at a lower tension force, because the shear stress in the interfaces exceeds their associated strength limits. Thus, it is assessed that the ANSYS model serves as a conservative estimate of the adhesive joint strength. The model can consequently be utilized to estimate the joint strength between the new rotor can and manacle ring.

2.2 Optimal Design of Composite Rotor Can

To yield the best possible solution, the design of the rotor can is set up as an optimal design problem.

2.2.1 Problem Definition

The rotor can is subjected to an internal pressure, and requirements regarding displacements have been defined in Section 1.3. Furthermore, since a CFRE is used, a failure criterion should be implemented to check the mechanical strength of the design. Since filament winding is the chosen manufacturing process, considerations regarding manufacturability should be implemented. To minimize mass, and thus minimize cost, minimum material use is desired.

2.2.2 Information Collection

To facilitate minimization of the rotor can mass, an expression for the mass is formulated:

$$m = V\rho \tag{1}$$

where m, V and ρ are the mass, volume and density of the rotor can respectively. To check the mechanical strength of the CFRE, the max. stress, max. strain and the Tsai-Wu failure criteria are used, where the latter is defined as:

$$F_i\sigma_i + F_{ij}\sigma_i\sigma_j = 1 \quad , \quad \{i,j\} = 1,2,\ldots,6 \tag{2}$$

where F_i and F_{ij} are first and second order strength tensors, and σ_i and σ_j are in-plane stresses. The criterion is utilized with the assumption of a state of plane stress, expressed as follows:

$$\begin{aligned} &F_1\sigma_1 + F_2\sigma_2 + F_6\sigma_6 + \cdots \\ &F_{11}\sigma_1^2 + F_{22}\sigma_2^2 + F_{66}\sigma_6^2 + 2F_{12}\sigma_1\sigma_2 = 1 \end{aligned} \tag{3}$$

where the subscript 1 and 2 correspond to the longitudinal and transverse in-plane directions, while subscript 6 corresponds to in-plane shear.
Due to geometrical restrictions, the inner radius of the existing rotor can is not to be altered. From the permitted maximum displacement u_{max} and the thickness of the existing rotor can, which is 0.4 mm, the sum of thickness and radial displacement for the new rotor can may not exceed 0.55 mm. Likewise, the minimum and maximum height of the rotor can are subjected to geometrical limitations of 116 mm and 136.5 mm respectively. The maximum height accounts for the maximum permitted axial displacement w_{max}. The mentioned restrictions are expressed as follows:

$$0 \leq n \cdot t + u_{max} \leq 0.55 \qquad \text{[mm]} \tag{4}$$

$$0 \leq n \cdot t + v_{max} \leq 0.55 \qquad \text{[mm]} \tag{5}$$

where n is the number of layers and t is the layer thickness, which is chosen to be equal for all layers. Additionally, manufacturability by use of filament winding is considered by enforcing geometrical convexity of the rotor can top and by limiting the fiber angles. In practice, the rotor can top is defined from four points, as shown in Fig. 10. Since the rotor can is axisymmetric, the top is created by revolving the spline around the z-axis. KP_0, denominated a keypoint, with fixed z-coordinate $z_0 = 116$ mm, is placed at the top of the cylindrical part of the rotor can. KP_1, KP_2 and KP_3 have variable z-coordinates, denominated z_1, z_2 and z_3. A cubic spline is used to interpolate a function between the four keypoints, which defines the geometry of the rotor can top.

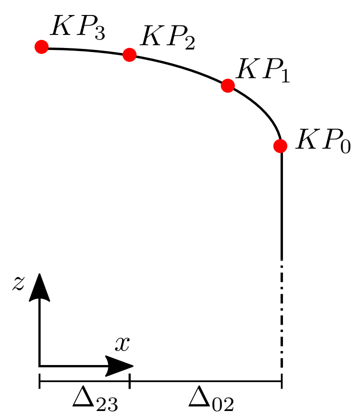

Fig. 10 Points used to define geometry and check geometrical convexity of rotor can top.

A central difference approximation is used to calculate the curvature at KP_2, which is enforced to be negative. Thus, the spline describing the shape of the rotor can top enforces the top of the rotor can to be geometrically convex. Additionally, the following relations for the z-coordinates z_1, z_2 and z_3 are defined using predefined constants c_1, c_2 and c_3:

$$116c_1 \leq z_1 \qquad [\mathrm{mm}] \tag{6}$$

$$c_2 z_1 \leq z_2 \qquad [\mathrm{mm}] \tag{7}$$

$$c_3 z_2 \leq z_3 \qquad [\mathrm{mm}] \tag{8}$$

$$z_3 \leq 136.5 - w_{max} \qquad [\mathrm{mm}] \tag{9}$$

$$\frac{z_3 - 2z_2 + z_0}{\Delta_{02}\Delta_{23}} \leq c_4 \qquad [\mathrm{mm}^{-1}] \tag{10}$$

Since the calculated curvature is approximate, a small negative contribution c_4 is added to ensure geometrical convexity. Restrictions for the fiber orientations are from [3, p. 86] defined as follows. An angle of 0° corresponds to the hoop direction of the rotor can:

$$-85 \leq \theta_i \leq 85 \qquad [^\circ] \tag{11}$$

where θ_i is the fiber orientation of the i^{th} layer and i is defined as:

$$i = 1, \ldots, \frac{n}{2} \qquad \text{for } n \text{ even} \tag{12}$$

$$i = 1, \ldots, \frac{n+1}{2} \qquad \text{for } n \text{ odd} \tag{13}$$

The above definition is utilized due to the desire of obtaining a regular anti-symmetric laminate. This is achieved by assigning fiber orientations to the layers as illustrated in Fig. 11. A regular anti-symmetric fiber layup is desired to reduce or avoid shear-extension, bending-extension and bend-twist coupling effects.

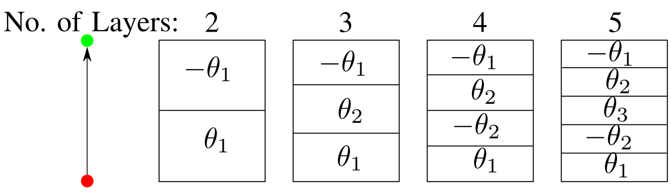

Fig. 11 Definition of fiber layup, where a regular anti-symmetric laminate is desired.

The laminate is defined from the inside of the rotor can, red dot, towards the outside of the rotor can, green dot. The above figure is for illustrative purposes and does not imply that the laminate thickness is independent of the number of layers utilized. Only the laminates with two and four layers are anti-symmetric. For the laminates with three and five layers to be anti-symmetric, it is required that the midlayer is either 0° or 90°. The layer thickness is defined to be within the following range:

$$0.10 \leq t \leq 0.12 \qquad [\mathrm{mm}] \tag{14}$$

From Eq. (4) and Eq. (14) the maximum number of layers is limited to five, while a lower limit of two layers is chosen:

$$2 \leq n \leq 5 \tag{15}$$

2.2.3 Definition of Design Variables

On the basis of the collected information, the following design variables are included in the optimization problem, with i as defined in Eq. (12) and Eq. (13).

$$n, \quad \theta_i, \quad t, \quad z_1, \quad z_2, \quad z_3 \tag{16}$$

2.2.4 Identification of Optimization Criterion

The cost function is dependent on the following design variables:

$$f(n, t, z_1, z_2, z_3) = m = V\rho \tag{17}$$

2.2.5 Identification of Constraints

Based on the information collected in Section 2.2.2, a total of at least 24 inequality constraints are defined. This number increases if more than two layers are used. The constraints are sorted into three different categories: Strength, stiffness & geometrical and manufacturing constraints, as shown in Tab. VII along with the number of constraints in each category. The index i assumes values as defined in Eq. (12) and Eq. (13).

Strength	Stiffness & Geometrical	Manufacturing
11	5	$7 + 2i$

Tab. VII Defined constraints sorted by category.

In total, j constraints are present, where j is defined as follows:

$$j = 23 + 2(i - 1) \tag{18}$$

where i assumes values as defined in Eq. (12) and Eq. (13).

2.3 Solution Method

On the basis of the defined optimization criterion and identified constraints, the optimization problem is solved by use of the genetic algorithm (GA) in MATLAB. The GA is utilized, since the number of layers n is defined as an integer variable. Furthermore, the fiber orientations θ_i are included as integer variables due to restrictions in manufacturing tolerances.

2.3.1 *Utilized Model*

To facilitate optimization of the rotor can design, an ANSYS finite element (FE) model is created. The model is discretized with quadratic solid elements, denominated SOLID186 in ANSYS. To ensure valid results with the solid model, 8.5×10^4 nodes are utilized in the discretization. An internal pressure of 1 MPa is applied. The rotor can is assumed to have all DOF locked at the bottom, where it is fixed with an adhesive. Since the model is going to be evaluated numerous times in the optimization algorithm, computational efficiency is desired. Thus, a second model is created, being discretized with quadratic shell elements, denominated SHELL281 in ANSYS. The element utilizes kinematic assumptions, which yield a simplification of the actual out-of-plane stress behaviour. Results obtained by use of the two models are compared to validate the use of the shell model.

To further improve computational efficiency, a convergence study is conducted with the shell model. The analysis yielded converged results for nodal displacements with 6×10^3 nodes. The utilized shell model is shown in Fig. 12, where the applied fixation is shown.

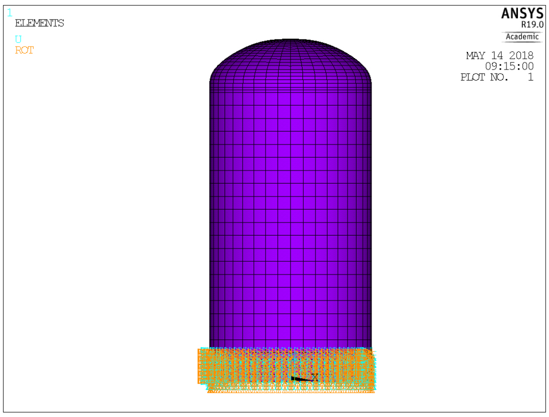

Fig. 12 Shell model showing the applied mesh and fixation.

To simplify the model and obtain further computational efficiency, the adhesive has not been included. Instead, the surface area covered by the adhesive has been fixed, locking all DOF. This implies that there will not occur any relative displacements between the manacle ring and rotor can. The simplification is deemed acceptable due to the manacle ring being much stiffer compared to the rotor can, including the assumption of a sufficiently stiff adhesive.

The hoop stresses calculated with the solid and shell models are compared in two parts of the rotor can: the cylindrical part as well as the transition between the cylindrical part and the top. The results yield a deviation of 0.1% in the cylindrical part of the rotor can. A small deviation in the in-plane stress distribution is observed in the transition. Here, the hoop stresses approximated by the shell model are 9.5% larger than the hoop stresses in solid model. Thus, the shell model yields more conservative results with respect to in-plane stresses. Furthermore, the calculated Tsai-Wu index is compared, as shown in Tab. VIII. The largest values are obtained at the layer on the inner surface, on the cylindrical part near the transition.

	Shell model	Solid model	Deviation [%]
Tsai-Wu Index [-]	0.71	0.65	9.2

Tab. VIII Tsai-Wu index for the shell model using SHELL281 elements and solid model using SOLID186 elements.

The shell model shows a larger value of the Tsai-Wu criterion compared to the solid model. It is thus concluded that the shell model generally yields conservative results. Hence, the shell model is deemed valid for use to solve the optimization problem.

3. Results

This section presents the results obtained by use of the methods presented in the previous section.

3.1 Design of Adhesive Joint

The adhesive joint of the redesigned rotor can is modeled on the basis of the model used for the conducted experiments. The adhesive joint is designed by use of a suitable adhesive, differing from the adhesive used in the experiments. The properties of the selected adhesive are listed in [4], including the effects of temperature and fatigue on the adhesive strength. Fig. 13 illustrates paths defined to plot the calculated interface and adhesive shear stresses from the ANSYS model. The calculated stresses are in-plane shear stresses, referring to the xz-plane as shown in the figure.

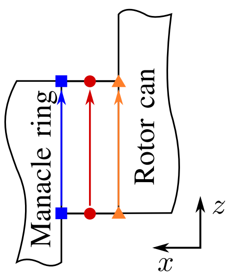

Fig. 13 Paths used to plot shear stresses shown in Fig. 14, using the same colour coding and marks.

The ultimate interface and adhesive shear strengths are calculated on the basis of the shear strength at 23°C. Subsequently, the decrease in strength due to temperature and fatigue is included. The increase in temperature from 23°C to 70°C is assumed to decrease the interface and adhesive shear strengths to approximately 75% of values at 23°C. From a rule of thumb for the selected adhesive stated in [5], the fatigue shear strength after 10^6 cycles is approximately equal to 30% of the static shear strength. The interface and adhesive shear stresses calculated in the FE model are plotted in Fig. 14. The approximated fatigue strengths at 70°C and 10^6 cycles are included as dotted lines. In the model, the rotor can is subjected to a tension force equal to the operational pressure. Thus, the effect of thermal load on the adhesive is ignored.

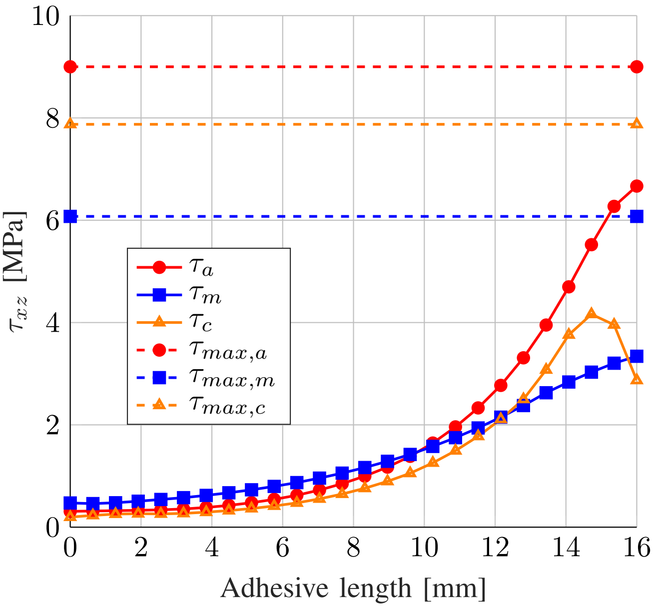

Fig. 14 Shear stresses in the xz-plane and ultimate shear strengths. τ_a, τ_m and τ_c denote shear stress at the adhesive midplane, manacle ring and rotor can interface respectively. $\tau_{max,a}$, $\tau_{max,m}$ and $\tau_{max,c}$ denote the corresponding approximated ultimate shear strengths.

The above figure shows that the shear stresses in the adhesive and in both of the interfaces are below each of their associated strength limits. Thus, the strength of the adhesive joint is deemed sufficient for the applied loading.
The decrease in shear stress at adhesive length equal to 15 mm is deemed to be due to interpolation of stresses in ANSYS when utilizing linear elements.

3.2 Optimal Design of Composite Rotor Can

To present the results of the optimization problem, Fig. 15 is used to define the constrained region of the sum of rotor can thickness and radial displacement, denominated u_{tot}.

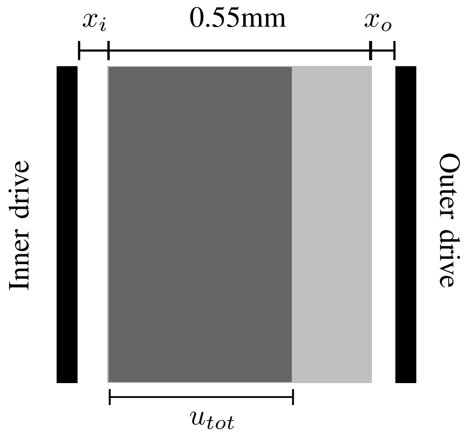

Fig. 15 Constraints for rotor can thickness and displacement. u_{tot} corresponds to the sum of rotor can thickness and displacement, where the maximum allowable value is defined as 0.55 mm. x_i and x_o correspond to the distance between the rotor can and the inner and outer drive respectively.

The light grey area on the above figure thus marks the distance which the outer drive can be moved closer to the inner drive. Fig. 16 shows the constrained region for shape optimization of the rotor can top. The distances marked with red illustrate the permitted z-coordinates for the points used to model the rotor can top.

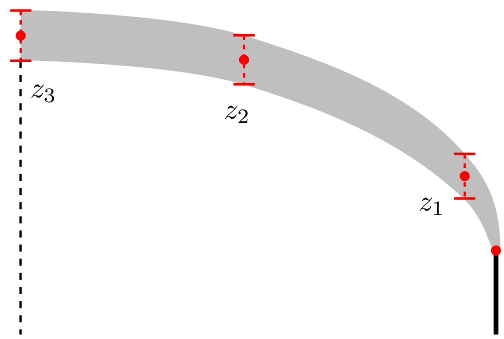

Fig. 16 Constraints for the shape of the rotor can top.

The GA is used with a population size of 20, 40 and 60, utilizing different initial guesses. This is done to establish the necessary population size, where the algorithm yields similar results when using different initial guesses. It was concluded that similar results were obtained with a population size of 60. The resulting design variables and the obtained minimum are shown in the following bullets:

- Mass: $m = 14.4$ g
- Number of layers: $n = 3$
- Fiber layup: $[-76°, 5°, 76°]$
- Layer thickness: $t = 0.1$ mm
- Rotor can top geometry:
  $\lfloor z_1\ z_2\ z_3 \rfloor^T = \lfloor 120.5\ 130.6\ 132.8 \rfloor^T$ mm

Furthermore, the sum of the resulting radial displacement and the rotor can thickness yielded $u_{tot} = 0.47$ mm. Regarding the fiber layup, the first value corresponds to the fiber orientation of the layer on the inside of the rotor can. The presented z-coordinates of the top geometry correspond to the lower bound of the constrained region presented in Fig. 16.

4. Conclusions

A new rotor can design was determined, being filament wound and fixed by adhesive bonding. The adhesive joint was designed on the basis of experimental results. Design of the rotor can was formulated as a minimum mass problem, resulting in a mass of 14.4 grams.

4.1 Answer to Research Question

Based on a static analysis, a composite solution for the rotor can has been designed in compliance with the listed requirements. Based on the dimensions of the new design and the calculated displacements, it is possible to move the outer magnetic drive 0.08 mm closer to the rotor can. This corresponds to a decrease of 2.4% relatively to the existing distance. With respect to the stated desire of obtaining a more efficient magnetic drive train, both the use of a composite rotor can and the possibility of reducing the distance between the magnetic drives contributes to fulfilling this desire. Regarding manufacturing cost of the rotor can, no definitive conclusion can be drawn due to the lack of information regarding specific manufacturing and material costs.

4.2 Future Work

For the composite rotor can solution to be complete, the following subjects must be investigated:

- Analysis of fatigue life
- Viscoelastic behaviour
- Temperature effects
- Sealing
- Estimation of unit cost

A static analysis of the rotor can has been conducted, but it will most likely fail in fatigue, why an analysis of the fatigue life should be conducted. A model incorporating thermal effects should be established, to validate the design of both the composite rotor can and the adhesive joint. The purpose of the rotor can is to seal the outer drive from the pumped media. Thus, the sealing properties of the chosen composite material should be investigated.

Acknowledgement

The authors of this work gratefully acknowledge Grundfos for sponsoring the 6th MechMan symposium.

References

[1] R. D. Cook, D. S. Malkus, M. E. Plesha, and R. J. Witt, “Concepts and Applications of Finite Element Analysis,” 2002, chapter 17.8.

[2] Huntsman, “Araldite2011,” https://tinyurl.com/Araldite2011, 2012, viewed: 30-04-2018.

[3] E. J. Barbero, “Introduction to composite materials design,” 2011.

[4] Huntsman, “Araldite AW4859-HW4859,” https://tinyurl.com/AralditeAW4859-HW4859, 2010, viewed: 27-04-2018.

[5] ——, “Users Guide to Adhesives,” https://www.freemansupply.com/datasheets/adhesivesguide.pdf, 2007, viewed: 04-05-2018.